Near-field Signal Model for Large-Scale Uniform Circular Array and Its Experimental Validation

Ji, Yilin; Fan, Wei; Pedersen, Gert F.

Published in:
I E E E Antennas and Wireless Propagation Letters

DOI (link to publication from Publisher):
10.1109/LAWP.2016.2629189

Publication date:
2017

Document Version
Accepted author manuscript, peer reviewed version

Near-field Signal Model for Large-Scale Uniform Circular Array and Its Experimental Validation

Yilin Ji, Wei Fan, Gert F. Pedersen

***Abstract*—The usually considered far-field assumption may not hold anymore, as the array aperture increases to a certain extent with respect to (w.r.t.) the near-field outer boundary (NFB), i.e. $R_{\text{NFB}} = 2D^2/\lambda$ with D being the array aperture and λ the wavelength. Under this circumstance, estimating channel parameters with the plane-wave model may result in severe error. In this paper, a near-field signal model was proposed for the uniform circular array (UCA) to avoid the plane-wave model mismatch during channel estimation at its near-field region. The ability of the underlying model to estimate path parameters were investigated with its ambiguity function. Moreover, a distance threshold dependent on the conventional NFB was proposed, and for the cases where the sources or the scatterers are located outside the proposed distance threshold, the plane-wave model could still be used with little estimation error.**

***Index Terms*—Large-scale uniform circular array, near-field signal model, near-field outer boundary, channel estimation.**

I. Introduction

In current channel models, the far-filed assumption is often adopted, since the antenna aperture is so small with respect to (w.r.t) the distance between the transmitter (Tx), the receiver (Rx) and the scatterers. However, this is changing rapidly for the upcoming fifth-generation (5G) network, with new essential features, such as large-scale antenna arrays, high frequency bands, small cellular coverage and close distance between Tx and Rx. With the increase of the array aperture, the corresponding near-field outer boundary (NFB) expands significantly. Therefore, the far-field assumption may not hold anymore. For example, a uniform linear array (ULA) of 8 elements with half-wavelength spacing operating at $2\,\text{GHz}$ has a NFB of $3.68\,\text{m}$, while a ULA of 100 elements with the same spacing operating at $30\,\text{GHz}$ has a NFB of about $49\,\text{m}$, which violates the far-field assumption in typical propagation environment for 5G deployment. Therefore, the signal model under near-field assumption, specifically the spherical-wave model, should be considered in this case to avoid the plane-wave model mismatch during channel estimation.

Estimation algorithms based on subspace [1], [2] and maximum likelihood [3], [4] were proposed for source localization purpose. Usually, the estimation performance is characterized by the Cramér-Rao bound (CRB), and the ambiguity function. The CRB indicates the local estimation error, while the ambiguity function shows the global resolution and large error properties [5]. In [6], [7], the CRB for channel parameters are derived under near-field condition. On the other hand, the plane-wave model, which has been widely accepted in industry and academia, has a lower complexity than the spherical-wave model. Thus, the plane-wave model is still often used to estimate the channel at the near field [8]–[10]. However, to which extent we can approach the signal from near-field region with the far-field model without significant estimation error is not thoroughly investigated.

Yilin Ji, Wei Fan, and Gert F. Pedersen are with the APNET section at the Department of Electronic Systems, Falculty of Engineering and Science, Aalborg University, Denmark. Email: {yilin, wfa, gfp}@es.aau.dk

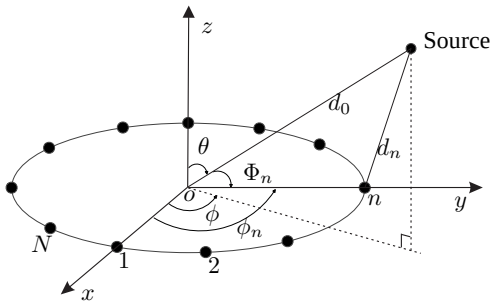

Fig. 1. Geometry of the incident wave from a source impinging upon an N-elemtent UCA in the rectangular coordinate.

In this paper, a UCA with sources located in its near-field region was considered. The estimation performance of channel parameters such as azimuth of arrival and distance d_0 from the source to the array (range) was investigated in terms of the ambiguity function of the array steering vector. Compared to the ULA, the UCA has a coverage of 360° in azimuth. In addition, the UCA has the property of geometric symmetry about its center, which makes the ambiguity function independent of azimuth of arrival. Moreover, the transition behaviour from the spherical-wave model to the plane-wave model was also investigated w.r.t. the estimation error of azimuth of arrival.

The main contributions of this paper are listed as follows.

- Factors affecting the distance d_0 resolution, i.e. the accuracy of the estimation in d_0, were investigated with the ambiguity function in terms of the curvature of impinging wavefront, the NFB R_{NFB}, and the array aperture D.
- A distance threshold dependent on the original NFB was proposed to determine whether the near-field assumption needs to be considered for channel estimation. The proposed threshold was also verified with a measurement conducted in an anechoic chamber.

II. Signal Model

As shown in Fig. 1, an N-element UCA of radius r is located in the x-y plane of the rectangular coordinate with the array center anchored at the origin o. The coordinate of the nth array element can be written as vector $\mathbf{v}_n = [r\cos\phi_n, r\sin\phi_n, 0]^{\text{T}}$, where $\phi_n = 2\pi\frac{(n-1)}{N}, n \in [1, N]$ is its azimuth angle, and $(\cdot)^{\text{T}}$ denotes the transpose operator. Similarly, the coordinate of the source is written as $\mathbf{v}_0 =$

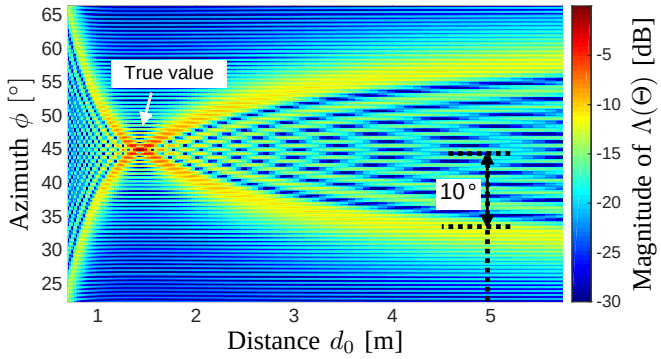

Fig. 2. The magnitude of $\Lambda(\Theta)$ in the ϕ-d_0 domain with θ fixed at 90° w.r.t. a synthetic UCA of 720 elements and radius $r = 0.5$ m at 30 GHz. The source was synthesized at $\theta' = 90°, \phi' = 45°$, and $d_0' = \sqrt{2}$ m.

$[d_0 \sin\theta\cos\phi, d_0 \sin\theta \sin\phi, d_0 \cos\theta]^{\mathrm{T}}$, where $\{\theta, \phi\}$ is the set of elevation and azimuth angle of the incident wave w.r.t. the array center. d_0, d_n are the distance from the source to the array center and the nth array element, respectively. Further, d_n can be expressed with d_0 as

$$d_n = \sqrt{r^2 + d_0^2 - 2rd_0 \cos\Phi_n}, \tag{1}$$

where Φ_n is the angle between the two vectors $\mathbf{v}_0$ and $\mathbf{v}_n$, with $\cos\Phi_n = \sin\theta\cos(\phi - \phi_n)$.

Considering the "source" as either the Tx or the scatterer in the environment, the array steering vector $\mathbf{s}(\Theta) = \{s_n(\Theta)\} \in \mathbb{C}^{N\times 1}$ corresponding to a single propagation path received at the UCA can be written as

$$s_n(\Theta) = \exp(-j2\pi f(d_n - d_0)/c), \tag{2}$$

where $\Theta = \{\theta, \phi, d_0\}$ is a vector consisting of the path parameters, i.e. the elevation of arrival θ, the azimuth of arrival ϕ, and the distance d_0 from the source to the array center. When the far-field assumption is considered, i.e. d_0 approaching infinity, the near-field steering vector (2) simplifies to

$$s_n(\theta, \phi) = \exp(-j2\pi f r \sin\theta\cos(\phi - \phi_n)/c). \tag{3}$$

For notation simplicity, $\mathbf{s}^{\mathrm{NF}}$ and $\mathbf{s}^{\mathrm{FF}}$ are used to denote the near-filed (NF) and the far-field (FF) steering vectors in (2) and (3), respectively, in the sequel.

III. Properties of the Array Steering Vector

A. Ambiguity function of the Array Steering Vector

The ambiguity function (also known as uncertainty function, or resolution function) was calculated with the array steering vector $\mathbf{s}^{\mathrm{NF}}$ to determine whether an arbitrary set of parameter $\Theta' = \{\theta', \phi', d_0'\}$ can be detected. The ambiguity function $\Lambda(\Theta)$ at frequency f is calculated as

$$\Lambda(\Theta : \Theta') = \frac{[\mathbf{s}^{\mathrm{NF}}(\Theta)]^{\mathrm{H}}\mathbf{s}^{\mathrm{NF}}(\Theta')}{\|\mathbf{s}^{\mathrm{NF}}(\Theta)\| \cdot \|\mathbf{s}^{\mathrm{NF}}(\Theta')\|}, \tag{4}$$

where $(\cdot)^{\mathrm{H}}$ denotes the complex conjugate operator, and $\|\cdot\|$ denotes the Euclidean norm. Fig. 2 shows the ambiguity function calculated with a synthetic source for a UCA. Note that the spacing between consecutive array elements should always be smaller than half wavelength to avoid spatial aliasing [11].

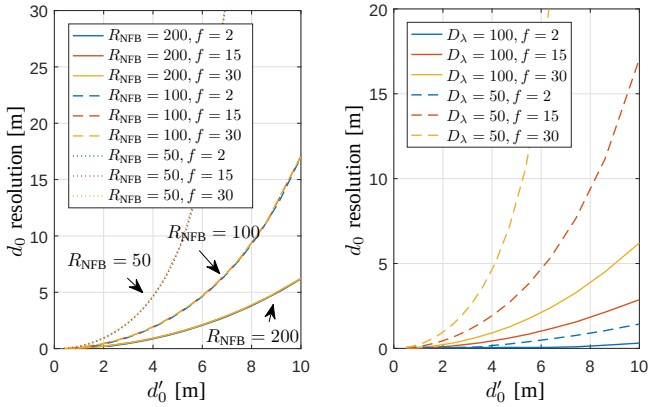

Fig. 3. The relation between d_0 resolution and d_0' calculated at $f = \{2, 15, 30\}$ GHz, $\theta = 90°$ with (a) $R_{\mathrm{NFB}} = \{50, 100, 200\}$ m, and (b) $D_\lambda = \{50, 100\}\,\lambda$. Units were omitted in the legends. Note that a smaller value of the resolution corresponds to a better performance.

In Fig. 2, the mainlobe of $\Lambda(\Theta)$ is very sharp, showing high accuracy of the estimates $\hat{\Theta}$. However, the crossing shape of the sidelobes indicates parameter ϕ and d_0 are not independent w.r.t. the ambiguity function, which means they should be jointly estimated to find the global maximum. Moreover, it can be seen that given $d_0 > d_0'$, huge error may appear in the estimate $\hat{\phi}$ (e.g. the angle estimation error $\mathrm{e}_{\hat{\phi}} \approx 10°$ at $d_0 = 5$ m). Since the far-field model can be considered as a special case of the near-field model with d_0 approaching infinity, estimating the near-field signal with the far-field model may also lead to significant angle estimation error. This model mismatch issue was further discussed in the following sections.

B. Factors Affecting the Resolution of the Distance d_0

The resolution of the distance d_0 is defined to be the width between the two points where $\Lambda(\Theta)$ decreases by 3 dB from its maxima in d_0 domain. Its value characterizes the estimation accuracy in d_0. In other words, the uncertainty of the estimate $\hat{d}_0$ increases with the width of the mainlobe of $\Lambda(\Theta)$. Thus, a smaller value of the resolution corresponds to a better performance. Factors affecting the d_0 resolution were studied w.r.t. the curvature of the impinging spherical wavefront, which can be calculated as $1/d_0$, the array aperture D, and the NFB R_{NFB}. Here we recall that $R_{\mathrm{NFB}} = 2D^2/\lambda$, where $D = 2r$ is the same as the diameter of the UCA. D in unit of wavelength is denoted as D_λ. The ambiguity function $\Lambda(\Theta)$ was calculated with specifically $R_{\mathrm{NFB}} = \{50, 100, 200\}$ m, $D_\lambda = \{50, 100\}\,\lambda$, $f = \{2, 15, 30\}$ GHz, and d_0' up to 10 m. Note that the radius r of the array is uniquely determined with R_{NFB}, D_λ, and f.

Fig. 3 shows the relation between d_0 resolution and d_0' w.r.t. different R_{NFB}, D_λ, and f at elevation $\theta = 90°$. Since the ability of the array to estimate d_0 is inherit from the curvature of the impinging wavefront, it is essential that the d_0 resolution increases with d_0'. Moreover, in Fig. 3(a), the curves of the d_0 resolution w.r.t. the same R_{NFB} at different f almost overlap with each other. In Fig. 3(b), the d_0 resolution decreases with D_λ but increases with f, causing the overall influence not so clear as that of R_{NFB}. The same relations at different elevations

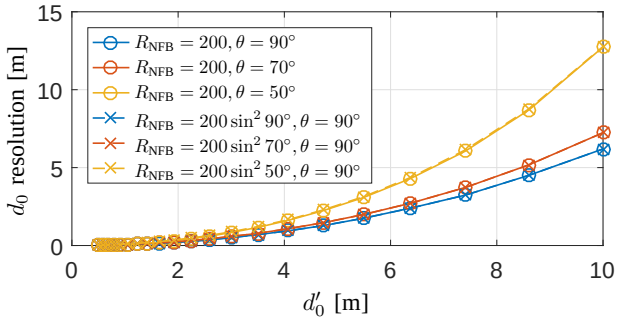

Fig. 4. The relation between d_0 resolution and d_0' calculated at elevation $\theta = \{50°, 70°, 90°\}$, $R_{\text{NFB}} = 200\,\text{m}$ ("$\circ$" marker); at $\theta = 90°$, $R_{\text{NFB}} = \{200\sin^2 50°, 200\sin^2 70°, 200\sin^2 90°\}\text{m}$ ("$\times$" marker).

are shown in Fig. 4. It is observed that the effect of elevation θ can be translated to R_{NFB} multiplied by a factor $\sin^2\theta$, i.e. once the d_0 resolution is determined at $\phi = 90°$, the d_0 resolution at other elevations can be determined by it with an effective NFB, $\sin^2\theta R_{\text{NFB}}$.

From the observation of Fig. 3 and 4, it can be inferred that the relation between d_0 resolution and d_0 is governed by the corresponding NFB independently of frequency. More specifically, given the same d_0, a smaller $\sin^2\theta R_{\text{NFB}}$ (equivalently a smaller $\sin^2\theta D_\lambda$ at a fixed frequency) results in a larger d_0 resolution, which leads to a less accurate estimate of d_0.

C. Transition from Near Field to Far Field

To investigate at which distance, the signal from near-field region can be estimated with far-field model without significant estimation error in ϕ, a one-wave scenario was synthesized with the near-field model $\mathbf{s}^{\text{NF}}$ at different distance d_0, and estimated with the far-field model $\mathbf{s}^{\text{FF}}$ with the classical (Bartlett) beamforming. Fig. 5 shows the estimation error $\text{e}_{\hat{\phi}}$ w.r.t. different R_{NFB} and d_0 at 30 GHz. Note that the obtained $\text{e}_{\hat{\phi}}$ is caused by the far-field model mismatch, so it is irrelevant to the estimation algorithm used [5]. Different elevations are considered and $\theta = \{70°, 90°\}$ are shown as examples. A clear boundary above which $\text{e}_{\hat{\phi}}$ converges to $0°$ can be seen, and further modelled with a linear equation (green line),

$$d_0 = \beta \cdot \sin^2\theta R_{\text{NFB}} + \gamma. \tag{5}$$

The obtained values for β and γ at $f = \{2, 15, 30\}$ GHz at $\theta = 90°$ were gathered in Table I, along with their mean values. It is shown the coefficient $\beta = 0.14$ is quite stable over a large span of frequency, and the bias γ is small and negligible compared to the first term in (5). As a result, since $\sin^2\theta \leq 1$, the product $(0.14R_{\text{NFB}})$ can be used as a distance threshold to decide whether it is necessary to deploy the near-field model for all elevations. This threshold is much more relaxed compared to the conventional NFB assumed in the literature [3], [12]. When d_0 is larger than this threshold, the far-field model can be used to lower the model complexity.

IV. Measurement Validation

A measurement campaign was conducted in an anechoic chamber to validate both the proposed near-field signal model

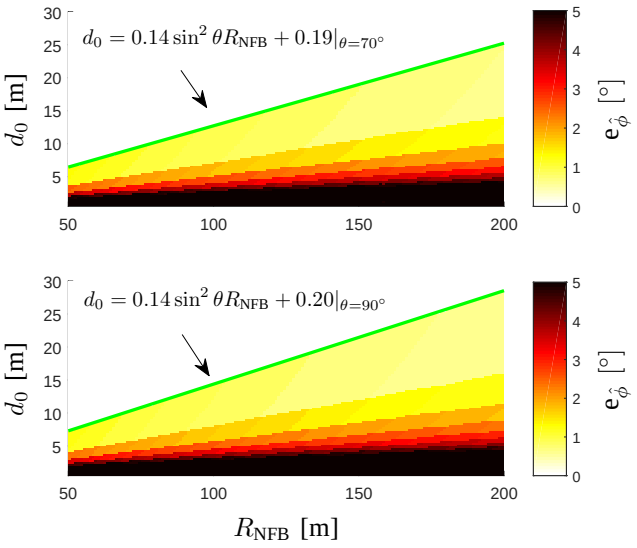

Fig. 5. Estimation error $\text{e}_{\hat{\phi}}$ at $\theta = 70°$ (top) and $\theta = 90°$ (bottom) w.r.t. $R_{\text{NFB}} \in [50, 200]$ m, and $d_0 \in [0.5, 30]$ m at 30 GHz. The color range was confined in $[0, 5]°$ to have a higher color sensitivity at small values.

TABLE I
Coefficient β and bias γ at 2, 15, 30 GHz, $\theta = 90°$.

f [GHz]	2	15	30	Mean
β	0.14	0.14	0.14	0.14
γ [m]	0.13	0.16	0.20	0.16

and the distance threshold $(0.14R_{\text{NFB}})$. The Tx was equipped with a directional horn antenna of 20° half-power beamwidth. On the Rx side, an omnidirectional biconical antenna was mounted on a turntable. A virtual UCA was realized via rotating the Rx antenna mechanically in $[0, 360]°$ in azimuth plane at 1° step, which resulted in 360 virtual elements. Both antennas on the Tx and the Rx side were vertically polarized, and placed at the same height. The channel frequency responses were measured at each element position with a vector network analyzer (VNA) from 28 to 29 GHz with 101 frequency points. The measurements were conudcted

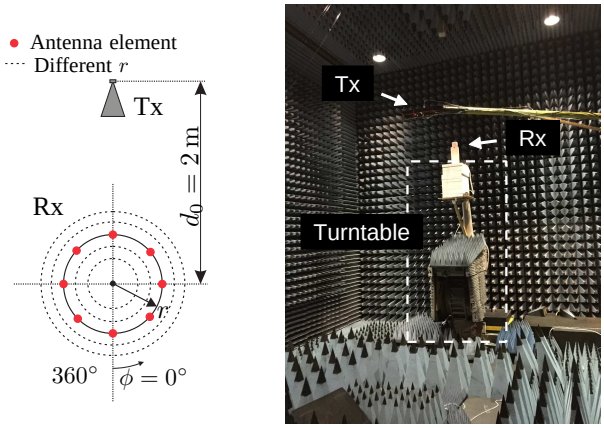

(a) (b)

Fig. 6. (a) The diagram and (b) photo of the measurement settings in the anechoic chamber. The distance from the Tx to the center of the Rx array is $d_0 = 2$ m. Measurement was done with different radius r.

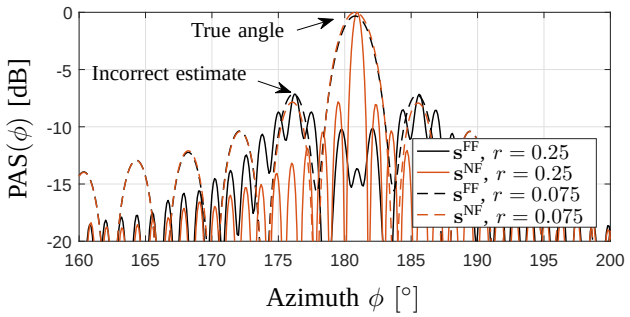

Fig. 7. The PAS(ϕ) calculated with $\mathbf{s}^{\mathrm{FF}}$ and $\mathbf{s}^{\mathrm{NF}}$. $r = \{0.075, 0.25\}$ m corresponding to $(0.14R_{\mathrm{NFB}}) = \{0.61, 6.77\}$ m at 29 GHz. $d_0 = 2$ m.

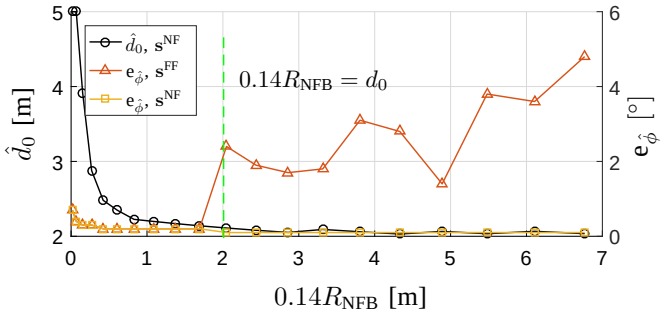

Fig. 8. The estimates $\hat{d}_0$ obtained with $\mathbf{s}^{\mathrm{NF}}$ (left y-axis) w.r.t. $0.14R_{\mathrm{NFB}}$, and the estimates error $\mathrm{e}_{\hat{\phi}}$ (right y-axis) obtained with both models. $0.14R_{\mathrm{NFB}} = d_0$ is shown in green dashed line.

with 20 different radius r of the UCA, which were uniformly selected in $[0.0125,\ 0.25]$ m, corresponding to R_{NFB} in $[0.12,\ 48.33]$ m at 29 GHz. The distance from the Tx to the Rx array center was fixed to $d_0 = 2$ m. Fig. 6 gives the diagram and the photo of the measurement settings, respectively.

The azimuth of arrival ϕ and the distance d_0 were estimated with the classical beamforming at 29 GHz. The far-field and the near-field models were considered respectively for measurement conducted at each r. Fig. 7 illustrates the obtained power angular spectrum PAS(ϕ) normalized to the measured signal power, at $r = \{0.075, 0.25\}$ m, corresponding to $0.14R_{\mathrm{NFB}} = \{0.61, 6.77\}$ m. For the case $d_0 > 0.14R_{\mathrm{NFB}}$ at $r = 0.075$ m, there is little difference between the PAS(ϕ) obtained from the far-field and the near-field model with ϕ estimated at about $181°$ (true angle). However, for the case $d_0 < 0.14R_{\mathrm{NFB}}$ at $r = 0.25$ m, the far-field model failed to estimate the true angle, with an estimation error of around $4°$. Moreover, the PAS(ϕ) of the far-field model is about 14 dB lower than that of the near-field model at about $\phi = 181°$, which shows the severity of the model mismatch when d_0 is smaller than $(0.14R_{\mathrm{NFB}})$.

In Fig. 8, the estimate $\hat{d}_0$ obtained with near-field model converges to the true value $d_0 = 2$ m, with the increase of R_{NFB}, which is consistent with the analysis given in Section III-B. The estimates error $\mathrm{e}_{\hat{\phi}}$ obtained with both models were also shown on the right y-axis. It can be seen that $\mathrm{e}_{\hat{\phi}}$ obtained with the near-field model (yellow line) is negligible, while $\mathrm{e}_{\hat{\phi}}$ obtained with the far-field model (red line) increases with R_{NFB} right to the proposed threshold, showing good conformity with the numerical analysis given in Section III-C.

V. Conclusion

In this paper, a generic near-field signal model for the UCA was proposed. The ability of the near-field model to estimate distance d_0 from the source was studied with the ambiguity function, and the d_0 resolution was found to be governed by the near-field outer boundary (NFB), i.e. R_{NFB}, independently of frequency. A distance threshold $(0.14R_{\mathrm{NFB}})$ was derived to decide whether the near-field model needs to be considered with a specific array size, frequency and scenario by comparing its value with d_0. For the case where d_0 is larger than this threshold, the plane-wave model can be used to estimate channel with little angle estimation error to achieve a lower model complexity. Both the proposed near-field model and the distance threshold were verified with the measurements conducted in an anechoic chamber.

Acknowledgment

This work was supported by the Innovation Fund Denmark via the Virtusuo Project. The work of Dr. Wei Fan was supported by the Financial assistance from the Danish council for Independent Research under Grant DFF 6111-00525. The authors appreciate the assistance from Mrs. Fengchun Zhang, Mr. Anders Karstensen and Mr. Kristian Bank on practical measurements.

References

[1] J. A. Cadzow, "Multiple Source Location - The Signal Subspace Approach," *IEEE Transactions on Acoustics, Speech, and Signal Processing*, vol. 38, no. 7, pp. 1110–1125, 1990.

[2] T. Hirano and N. Kikuma, "Location Estimation of Multiple Near-Field Broadband Sources by Combined Use of DOA-Matrix Method and SAGE Algorithm in Array Antenna Processing," *Proceedings of ISAP2012, Nagoya, Japan*, pp. 363–366, 2012.

[3] J. Chen, S. Wang, and X. Yin, "A Spherical-Wavefront-Based Scatterer Localization Algorithm using Large-Scale Antenna Arrays," *IEEE Communications Letters*, vol. 7798, no. c, pp. 1–1, 2016.

[4] K. Haneda, J. I. Takada, and T. Kobayashi, "A parametric UWB propagation channel estimation and its performance validation in an anechoic chamber," *IEEE Transactions on Microwave Theory and Techniques*, vol. 54, no. 4, pp. 1802–1811, 2006.

[5] M. J. D. Rendas and J. M. F. Moura, "Ambiguity in Radar and Sonar," *IEEE Transactions on Signal Processing*, vol. 46, no. 2, pp. 294–305, 1998.

[6] A. J. Weiss and B. Friedlander, "Range and Bearing Estimation Using Polynomial Rooting," *IEEE Journal of Oceanic Engineering*, vol. 18, no. 2, pp. 130–137, 1993.

[7] J. P. Delmas and H. Gazzah, "CRB analysis of near-field source localization using uniform circular arrays," *ICASSP, IEEE International Conference on Acoustics, Speech and Signal Processing - Proceedings*, pp. 3996–4000, 2013.

[8] X. Gao, O. Edfors, F. Rusek, and F. Tufvesson, "Massive MIMO Performance Evaluation Based on Measured Propagation Data," *IEEE Transactions on Wireless Communications*, vol. 14, no. 7, pp. 3899–3911, 2015.

[9] W. Fan, I. Carton, J. Ø. Nielsen, K. Olesen, and G. F. Pedersen, "Measured wideband characteristics of indoor channels at centimetric and millimetric bands," *EURASIP Journal on Wireless Communications and Networking*, vol. 2016, no. 1, p. 58, 2016.

[10] F. Zhang, W. Fan, and G. F. Pedersen, "Frequency Invariant Uniform Circular Array for Wideband mm-Wave Channel Characterization," vol. 1225, no. 2, pp. 1–4, 2016.

[11] D. H. Johnson and D. E. Dudgeon, *Array signal processing: concepts and techniques*. Simon & Schuster, 1992.

[12] S. Wu, C. X. Wang, E. H. M. Aggoune, M. M. Alwakeel, and Y. He, "A non-stationary 3-D wideband twin-cluster model for 5G massive MIMO channels," *IEEE Journal on Selected Areas in Communications*, vol. 32, no. 6, pp. 1207–1218, 2014.